Pergamon

Int. J. Solids Structures Vol. 34, No. 1, pp. 1–17, 1997

0020-7683/97 $15.00 + .00

0020-7683(95)00289-8

CRACKS IN FUNCTIONALLY GRADED MATERIALS

PEI GU and R. J. ASARO
Department of Applied Mechanics and Engineering Sciences,
University of California at San Diego, La Jolla, CA 92093-0411, U.S.A.

(*Received* 25 *October* 1995; *in revised form* 13 *November* 1995)

Abstract—A semi-infinite crack in a strip of an isotropic, functionally graded material under edge loading and in-plane deformation conditions is analyzed. Mixed mode stress intensity factors are analytically solved for up to a numerically determined parameter. The effects of material gradients on the mode I and mode II stress intensity factors and the phase angle used to measure mode mixity are determined. The solution is extended to the case where the strip is made of an orthotropic, functionally graded material. These results are applied to solve a four-point bending specimen configuration that may be used to test the fracture behavior of functionally graded materials. The nature of the crack tip fields and possible fracture criterion for functionally graded materials are discussed. Copyright © 1996 Elsevier Science Ltd

1. INTRODUCTION

Functionally graded materials (FGMs) to be used as, *inter alia*, superheat-resistive materials have promised attractive applications in furnace liners, space structures, and fusion reactors. FGMs consist of two distinct material phases, such as ceramic and metal alloy phases, and are the mixture of them such that the composition of each changes continuously along one direction. The change in microstructure induces chemical, material, and microstructural gradients, and makes functionally graded materials different in behavior from homogeneous materials and traditional composite materials (Yamanouchi *et al.*, 1990; Holt *et al.*, 1993). These materials are tailorable in their properties *via* the design of the gradients in chemistry and microstructure that is possible within them.

Experiments have shown that cracks occur in functionally graded materials (see above references) although the absence of sharp interfaces does alleviate problems with interface fracture. For cracks in this type of material, stress intensity factors are affected by the material gradients. Moreover, the fracture modes of the cracks in FGMs are inherently mixed when they are not parallel to the direction of material property variation, *i.e.*, there are typically both normal and shear tractions ahead of the crack tips because of the non-symmetry in the material properties. To characterize the material, fracture toughness data is required. To obtain the fracture toughness data, stress intensity factors for specimens subjected to variable external loads are needed. Most previous works on FGM crack configurations have concentrated on finite crack problems, *e.g.*, Delale and Erdogan (1983, 1988) and Noda and Jin (1993) have analyzed a finite crack in a plate subjected to mechanical and thermal loads. A semi-infinite crack in an interlayer between two dissimilar materials was considered by Yang and Shih (1994), and they obtained an approximate solution from a known bimaterial solution. We consider herein a semi-infinite crack in a strip of an isotropic, functionally graded material under edge loading and in-plane deformation conditions. Stress intensity factors for the crack tip are obtained. The solution is analytical up to a parameter which is obtained numerically. The solution is extended to the case where the strip is made of an orthotropic, functionally graded material. The results are applied to analyze a four-point bending specimen configuration that may be used to test the fracture behavior of functionally graded materials. The mode III stress intensity factor in the cracked plate subjected to anti-plane deformation is obtained. The nature of the crack tip fields and possible fracture criterion for functionally graded materials are discussed.

The main emphasis here is to analyze fracture behavior in materials that possess continuously graded microstructures. On the other hand, the physical picture developed for the cracked microstructure actually provides a more realistic model for cracks along interfaces, in general, at least for those that have any but atomic-scale width.

2. FIELD EQUATIONS FOR ISOTROPIC MEDIA

In this study, we take the elastic properties to be of following exponential forms

$$E'(y) = E_0 \, e^{\gamma y},$$
$$\nu'(y) = \nu_0(1+\varepsilon y)\, e^{\gamma y}, \tag{1}$$

where γ and ε are material constants representing the material gradients; E_0 and ν_0 are the values of these elastic properties at $y = 0$. For plane stress problems, $E'(y) = E(y)$ and $\nu'(y) = \nu(y)$, where $E(y)$ and $\nu(y)$ are Young's modulus and Poisson's ratio, respectively; for plane strain problems, $E'(y) = E(y)/[1-\nu(y)^2]$ and $\nu'(y) = \nu(y)/[1-\nu(y)]$. The parameters γ and ε have a dimension $[\text{length}]^{-1}$. These forms for the material properties have been previously used by Delale and Erdogan (1988) and Noda and Jin (1993); they provide, on the one hand, analytical flexibility and yet lead to somewhat simple forms for the field equations. The shear modulus, $\mu(y)$, relates to Young's modulus and Poisson's ratio by

$$\mu(y) = \frac{E'(y)}{2[1+\nu'(y)]}. \tag{2}$$

Using (1) and (2), the stress function $\Phi(x, y)$ defined in the same way as that for homogeneous materials, *i.e.*, stresses are obtained from the second derivatives of the stress function, satisfies the following equation

$$\frac{\partial^4\Phi}{\partial x^4} + 2\frac{\partial^4\Phi}{\partial x^2\,\partial y^2} + \frac{\partial^4\Phi}{\partial y^4} - 2\gamma\frac{\partial}{\partial y}\left(\frac{\partial^2\Phi}{\partial x^2} + \frac{\partial^2\Phi}{\partial y^2}\right) + \gamma^2\frac{\partial^2\Phi}{\partial y^2} = 0. \tag{3}$$

For a traction problem, the solution satisfies (3) and boundary conditions. The material constant γ enters the stress field of the traction problem, whereas the other material parameters E_0, ν_0 and ε do not. In (3), the fourth-order differential terms do not involve γ, and constitute the biharmonic equation, which is the equation for homogeneous materials.

By dimensional analysis, the stress field has the following generic form

$$\sigma_{ij}(x, y) = T\sigma_{ij}^{*}\left(\gamma h, \frac{\mathscr{L}}{h}, \frac{x}{h}, \frac{y}{h}\right), \tag{4}$$

where $i, j = 1, 2$; T is a representative stress magnitude; h is a characteristic length in the problem; $\mathscr{L}$ is the group of lengths which represents the geometry of the problem. This differs from the case of a homogeneous material in which material properties do not enter the stress field of a traction problem, and also differs from the case of a bimaterial in which Dundurs' parameters (Dundurs, 1969) measuring the material mismatch enter the stress field of a traction problem.

The parameters γh in the solution is dependent on the thickness of a functionally graded material, L, the Young's moduli at the upper and the lower boundaries of the material, E_u' and E_l', and the characteristic length, h. From (1),

$$\gamma h = \frac{h}{L} \ln \frac{E'_u}{E'_l}. \tag{5}$$

It is seen that γh is proportional to h/L, and increases logarithmically with the ratio of the two Young's moduli. For example, if $h/L = 1$, $\gamma h = 0.35$ for $E'_u/E'_l = 0.5$, and $\gamma h = 0.97$ for $E'_u/E'_l = 7$. The choice of h is arbitrary. If h_1 and h_2 denote two choices for the characteristic length, the corresponding stresses obtained satisfy the relation

$$\sigma^{*1}_{ij}\left(\gamma h_1, \frac{\mathscr{L}}{h_1}, \frac{x}{h_1}, \frac{y}{h_1}\right) = \sigma^{*2}_{ij}\left(\gamma h_2, \frac{\mathscr{L}}{h_2}, \frac{x}{h_2}, \frac{y}{h_2}\right). \tag{6}$$

3. CRACK TIP FIELDS

A brief review of the crack tip fields in functionally graded materials is given in this section. Consider a crack in a strip of a functionally graded material, as illustrated in Fig. 1. Stresses near the crack tip have a square-root singularity, and singular terms of the stresses (Jin and Noda, 1994) are of the form

$$\sigma_{ij} = \frac{K_{\mathrm{I}}}{\sqrt{2\pi r}} \bar{\sigma}^{\mathrm{I}}_{ij}(\theta) + \frac{K_{\mathrm{II}}}{\sqrt{2\pi r}} \bar{\sigma}^{\mathrm{II}}_{ij}(\theta) + \frac{K_{\mathrm{III}}}{\sqrt{2\pi r}} \bar{\sigma}^{\mathrm{III}}_{ij}(\theta), \tag{7}$$

where $i, j = 1, 2$; r and θ are the polar coordinates shown in Fig. 1. The dimensionless angular functions $\bar{\sigma}^{\mathrm{I}}_{ij}(\theta)$, $\bar{\sigma}^{\mathrm{II}}_{ij}(\theta)$ and $\bar{\sigma}^{\mathrm{III}}_{ij}(\theta)$ are the same as those for homogeneous materials. This can be easily proved by expanding the stress function as $\Sigma_{i=0} r^{i+\rho} \Phi_i(\theta, \gamma)$, and substituting the series into (3). The resulting equation for $\Phi_0(\theta, \gamma)$ and the eigen-value problem used to determine ρ do not involve γ and are the same as those for homogeneous materials. In fact, for any form of material properties and any orientation of the crack, the highest order differential terms in the equation which the stress function satisfies are the three fourth-order differential terms which constitute the biharmonic equation, and the terms in the equation involving material gradients are the lower order differential terms. These lead to that the equations for $\Phi_0(\theta, \gamma)$ and ρ are the same as those for homogeneous materials. The stress intensity factors K_{I}, K_{II} and K_{III} are functions of the material gradients, external load, and geometry. Material gradients do not affect the order of the singularity and the angular functions, but do affect the stress intensity factors. As a result the near-tip stresses have the same form as that for a homogeneous material. For an interface crack, stresses have an oscillatory singularity, and both the stress intensity factors and angular functions involve Dundurs' parameters, *i.e.*,

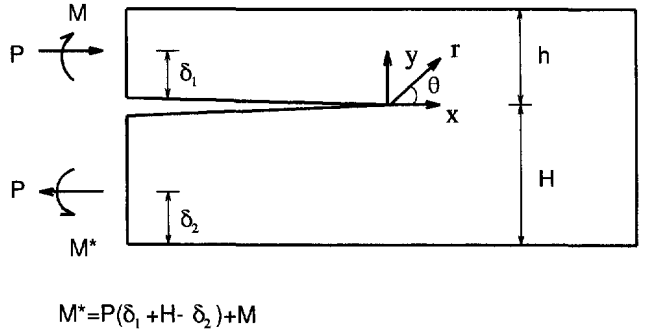

Fig. 1. A semi-infinite crack in a strip of a functionally graded material subjected to edge loading.

$$\sigma_{ij} = \frac{\mathrm{Re}(Kr^{i\varepsilon})}{\sqrt{2\pi r}}\tilde{\sigma}_{ij}^{\mathrm{I}}(\theta,\varepsilon) + \frac{\mathrm{Im}(Kr^{i\varepsilon})}{\sqrt{2\pi r}}\tilde{\sigma}_{ij}^{\mathrm{II}}(\theta,\varepsilon) + \frac{K_{\mathrm{III}}}{\sqrt{2\pi r}}\tilde{\sigma}_{ij}^{\mathrm{III}}(\theta), \tag{8}$$

where $K = K_{\mathrm{I}} + iK_{\mathrm{II}}$ is complex stress intensity factor, and

$$\varepsilon = \frac{1}{2\pi}\ln\frac{1-\beta}{1+\beta}. \tag{9}$$

In (9), β is one of the two Dundurs' parameters. The Dundurs' parameters, α and β, are defined as

$$\alpha = \frac{\mu_1(\kappa_2+1) - \mu_2(\kappa_1+1)}{\mu_1(\kappa_2+1) + \mu_2(\kappa_1+1)},$$
$$\beta = \frac{\mu_1(\kappa_2-1) - \mu_2(\kappa_1-1)}{\mu_1(\kappa_2+1) + \mu_2(\kappa_1+1)}, \tag{10}$$

where μ_1 and μ_2 are the shear moduli of the two bulk materials; $\kappa_i = 3-4\nu_i$ for plane strain and $\kappa_i = (3-\nu_i)/1+\nu_i)$ for plane stress ($i = 1, 2$), with ν_1 and ν_2 being the Poisson's ratios of the two bulk materials. It is noted that, by considering material gradients near the tip of an interface crack, the oscillatory behavior is removed, and the angular functions become independent of material properties. In this sense, the solutions presented here represent a more physically acceptable description of interface crack tip fields, at least for interfaces that have a finite width.

The strains obtained from the stresses given in (7) are

$$\varepsilon_{ij} = S_{ijkl}(0)\sigma_{kl} + [S_{ijkl}(y) - S_{ijkl}(0)]\sigma_{kl}, \tag{11}$$

where $S_{ijkl}(y)$ is the compliance tensor, and $S_{ijkl}(0)$ is the tensor at the crack tip. The second term in the above equation is in the order of $r^{3/2}$. So the singular strain field is

$$\varepsilon_{ij} = S_{ijkl}(0)\sigma_{kl}. \tag{12}$$

From (12), one is able to show that the near-tip displacement field is the same as that for the homogeneous materials.

From (7), the traction at the distance r ahead of the crack tip is

$$\sigma_{yy} + i\sigma_{xy} = \frac{K}{\sqrt{2\pi r}} \tag{13}$$

for an in-plane problem. For a mode III problem, the traction is, likewise,

$$\sigma_{yz} = \frac{K_{\mathrm{III}}}{\sqrt{2\pi r}}. \tag{14}$$

Having the near tip stress and displacement fields, the energy release rate of the crack tip is obtained as

$$\mathcal{G} = \frac{K_{\mathrm{I}}^2}{E'(0)} + \frac{K_{\mathrm{II}}^2}{E'(0)} + \frac{K_{\mathrm{III}}^2}{2\mu(0)}, \tag{15}$$

where $E'(0)$ and $\mu(0)$ are the Young's modulus and the shear modulus at the crack tip, respectively. It can be seen that the above eqns, (7) and (12)–(15), are independent of the forms of the material properties and the orientation of the crack, and they all have the

same forms as those for homogeneous materials. The path-independence of the J integral (Rice, 1968) holds if the crack is perpendicular to the direction along which material properties change; this is implied in Rice's original proof for homogeneous materials. Using the near tip fields obtained above, it can be shown that the J integral is equal to the energy release rate for the crack perpendicular to the direction along which material properties change.

The complex stress intensity $K = K_{\mathrm{I}} + iK_{\mathrm{II}}$ for FGMs has the following generic form

$$K = |K| \, \mathrm{e}^{i\psi}, \tag{16}$$

where

$$\psi = \tan^{-1} \frac{K_{\mathrm{II}}}{K_{\mathrm{I}}} \tag{17}$$

is the phase angle of the complex stress intensity factor. The phase angle measures mode mixity, *i.e.*, the proportion of the shear traction to the normal traction ahead of the crack tip, since

$$\psi = \tan^{-1} \left(\frac{\sigma_{xy}}{\sigma_{yy}} \right)_{\theta = 0, r \to 0}. \tag{18}$$

As a result of the regular singularity, this, again, is consistent with the phase angle defined for cracks in homogeneous materials. In the case of interface cracks, a material length is needed to define the phase angle.

As a starting point, we postulate that the crack starts to propagate when the energy release rate reaches a critical value Γ, the *toughness* of the FGM. The toughness is likely dependent on the material gradients, the position of the crack tip, namely h/H for the configuration shown in Fig. 1, and the mode mixity ψ. It is also possibly dependent on the propagation direction $\phi (-\pi < \phi < \pi)$ which is the angle between the propagation direction and the x axis in Fig. 1. The energy release rate is a function of the external load, elastic constants, the angle ϕ and the mode mixity ψ. Now, the fracture criterion is stated as

$$\mathscr{G} = \Gamma, \quad \frac{\partial}{\partial \phi} (\mathscr{G} - \Gamma) = 0. \tag{19}$$

The criterion also determines the propagation direction (kink angle). If toughness in the direction $\phi \neq 0$ is relatively larger than that in the direction $\phi = 0$, the crack would propagate along its original orientation. In this case, the fracture criterion is

$$\mathscr{G} = \Gamma \left(\frac{h}{H}, \psi \right), \tag{20}$$

where $\Gamma(h/H, \psi)$ is the toughness along the direction $\phi = 0$. The toughness of FGMs may be measured by experiments or obtained from micromechanics by considering their microstructures.

4. THE IN-PLANE PROBLEM

The in-plane crack problem is illustrated in Fig. 1, where a semi-infinite crack in a strip occupies the negative x axis and the crack tip is at the origin. The material properties change along the y axis. The geometry is specified by h, the distance between the crack face and the upper boundary, and H, the distance between the crack face and the lower boundary. The body extends infinitely in both the positive and negative x axes, and is loaded at the

left side far behind the crack tip. The deformation far behind the crack tip consists of bending and compression in the upper arm, and bending and tension in the lower arm. The external load results in two forces which are of the same magnitude P but which act in opposite directions, and two bending moments, M and M^*. The compressive and tensile forces act at the neutral axes of the upper and lower arms, respectively. One of the two moments, M, is given independently, and the other is $M^* = M + P(\delta_1 + H - \delta_2)$ by equilibrium, where δ_1 is the distance between the neutral axis of the upper arm and the crack face and δ_2 is the distance between the neutral axis of the lower arm and the lower boundary. According to the small-strain compatibility equations, the only non-zero strain, ε_{xx}, in the two arms far behind the crack tip varies linearly along the y axis.

We consider bending deformation in the two arms far behind the crack tip resulting from the two bending moments. The strain ε_{xx} can be expressed as

$$\varepsilon_{xx} = -\kappa(y - \delta_1) \tag{21}$$

in the upper arm, where κ is the curvature of the upper arm. The moment M relates to the curvature by

$$M = \kappa E_0 I_1. \tag{22}$$

In (22), I_1 is the moment of inertia and is given by

$$I_1 = \int_0^h e^{\gamma y}(y - \delta_1)^2 \, dy = \frac{h^3}{12}\alpha_1(\gamma h), \tag{23}$$

where

$$\alpha_1(\gamma h) = 12\left[\frac{1}{\gamma h}\left(1 - \frac{\delta_1}{h}\right)^2 e^{\gamma h} - \frac{2}{(\gamma h)^2}\left(1 - \frac{\delta_1}{h}\right)e^{\gamma h} + \frac{2}{(\gamma h)^3}e^{\gamma h} - \frac{1}{\gamma h}\left(\frac{\delta_1}{h}\right)^2 - \frac{2}{(\gamma h)^2}\frac{\delta_1}{h} - \frac{2}{(\gamma h)^3}\right]. \tag{24}$$

When $\gamma = 0$, $\alpha_1 = 1$ so that $I_1 = h^3/12$, a standard result for homogeneous materials. The only non-zero stress in the arm is the normal stress in the cross section,

$$\sigma_{xx} = -\frac{M(y - \delta_1)}{I_1} e^{\gamma y}. \tag{25}$$

By the equilibrium requirement $\int_0^h \sigma_{xx} \, dy = 0$, the position of the neutral axis is obtained as

$$\frac{\delta_1}{h} = \frac{\gamma h e^{\gamma h} - e^{\gamma h} + 1}{\gamma h(e^{\gamma h} - 1)}. \tag{26}$$

Similarly, results for the lower arm are

$$\sigma_{xx} = \frac{M^*(y + H - \delta_2)}{I_2} e^{\gamma h},$$

$$I_2 = \int_0^H e^{\gamma(h-H)}(y - \delta_2)^2 \, dy = \frac{H^3}{12}\alpha_2,$$

$$\frac{\delta_2}{H} = \frac{\gamma H e^{\gamma H} - e^{\gamma H} + 1}{\gamma H(e^{\gamma H} - 1)}, \tag{27}$$

where

$$\alpha_2(\gamma H) = \alpha_1(\gamma H)\,\mathrm{e}^{-\gamma H}. \tag{28}$$

We next consider axial deformation in the two arms resulting from the two forces. Since the compressive force acts on the neutral axis of the upper arm, the deformation caused by it is uniform compression. The stress distribution in the cross section to produce the uniform compression is

$$\sigma_{xx} = -\frac{P\gamma}{\mathrm{e}^{\gamma h}-1}\mathrm{e}^{\gamma y}. \tag{29}$$

Similarly, the stress distribution in the cross section of the lower arm due to the tensile force is

$$\sigma_{xx} = \frac{P_\gamma}{1-\mathrm{e}^{-\gamma H}}\mathrm{e}^{\gamma y}. \tag{30}$$

It is seen that in the cross sections the strains vary linearly with y, whereas the stresses vary exponentially with y. Expressions for the stresses and strains for the case that material properties change linearly along the y axis have been derived by Freund (1993) and Giannakopoulos *et al.* (1994) in studying thermal and mechanical responses in a compositionally graded layer sandwiched between two dissimilar materials without cracks, where a linear stress distribution along the thickness of the compositionally graded layer is obtained from the linear variation of material properties. Giannakopoulos *et al.* (1994) have also investigated plastic deformation in the compositionally graded layer. More recently Maewal *et al.* (1995) have developed a more general framework for analyzing thermally induced stresses in generally orthotropic FGMs with arbitrary gradients.

Having the remote field, the complex stress intensity factor K is obtained by the application of the J integral, dimension analysis and linearity consideration. The procedure is similar to that in Suo and Hutchinson (1990) for an interface crack. The complex stress intensity factor is obtained as

$$K = K_{\mathrm{I}} + iK_{\mathrm{II}} = \frac{1}{\sqrt{2}}\left(\sqrt{\frac{A}{h}}P - i\,\mathrm{e}^{i\varphi}\sqrt{\frac{I}{h^3}}M\right)\mathrm{e}^{i\omega}, \tag{31}$$

where

$$A = \gamma h\left(\frac{1}{\mathrm{e}^{\gamma h}-1} + \frac{1}{1-\mathrm{e}^{-\gamma H}}\right) + \frac{12}{\alpha_2}\left(\frac{h}{H}\frac{\delta_1}{h} + 1 - \frac{\delta_2}{H}\right)^2\frac{h}{H},$$

$$I = \frac{12}{\alpha_1} + \frac{12}{\alpha_2}\left(\frac{h}{H}\right)^3,$$

$$\sin\varphi = \frac{12}{\alpha_2\sqrt{AI}}\left(\frac{h}{H}\frac{\delta_1}{h} + 1 - \frac{\delta_2}{H}\right)\left(\frac{h}{H}\right)^2. \tag{32}$$

In (31), $\omega = \omega(\gamma h, h/H)$ is to be determined, and is in the range $0 \leqslant \omega \leqslant \pi/2$. The complex stress intensity factor is fully obtained apart from the dimensionless real scalar $\omega(\gamma h, h/H)$. The expression for K has a similar form as that for an interface crack. In the interface crack case, Dundurs' parameters enter the solution as variables of A, I, φ and ω, whereas the material constant γ enters the solution as a variable of those parameters in our case.

To determine $\omega(\gamma h, h/H)$, we solve the full boundary value problem for given γh and h/H, using the integral equation method. Integral equations for this problem can be obtained by Fourier transforms. The numerical procedure is to distribute dislocation densities simulating opening and sliding displacements of the crack in terms of Chebyshev polynomials,

Table 1. $\omega(\gamma h, h/H)$ (in degrees)

	γh											
h/H	0.2	0.4	0.6	0.8	1.0	1.2	1.4	1.6	1.8	2.0	2.2	2.4
0.0	53.8	54.9	56.0	56.9	57.5	58.0	58.3	58.5	58.6	58.6	58.5	58.4
0.1	53.5	54.8	56.0	56.9	57.5	58.0	58.3	58.5	58.6	58.6	58.5	58.4
0.5	51.6	52.4	53.2	54.0	54.7	55.3	55.9	56.4	56.8	57.1	57.4	57.5
1.0	49.6	50.1	50.7	51.2	51.7	52.2	52.7	53.1	53.5	53.8	54.1	54.4
2.0	47.0	47.3	47.6	47.9	48.2	48.5	48.8	49.1	49.4	49.6	49.9	50.2
10	40.8	40.9	40.9	41.0	41.1	41.2	41.2	41.3	41.4	41.5	41.6	41.7
100	39.0	39.0	39.0	39.1	39.1	39.1	39.1	39.1	39.1	39.1	39.1	39.1

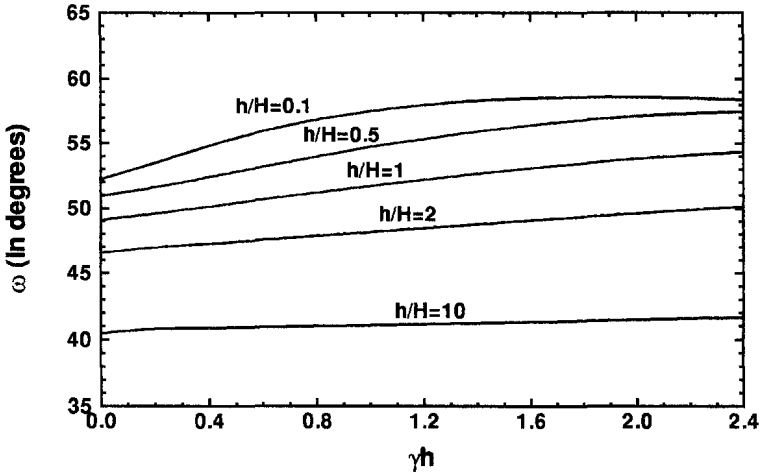

Fig. 2. Numerical results for $\omega(\gamma h, h/H)$.

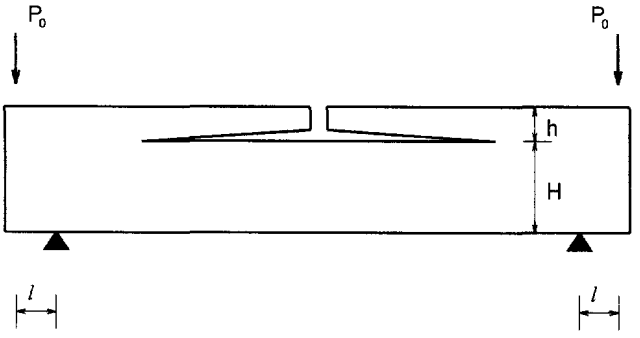

Fig. 3. A four-point bending specimen.

and to adjust the coefficients of these polynomials to satisfy the integral equations which are expressions of equilibrium (see Thouless *et al.*, 1987). Table 1 gives numerical results for ω when $0 \leqslant \gamma h \leqslant 2.4$ and $h/H = 0$, 0.1, 0.5, 1, 2, 10 and 100, which are also shown in Fig. 2. For most cases, the ω increases as γh increases, and the increase is larger for smaller h/H. For $h/H = 100$, the numerical solution shows little change of ω when γh varies between 0 and 2.4.

When $M = 0$, the phase angle $\psi = \omega$; when $P = 0$ (double-cantilever beam), $\psi = \omega + \varphi - 90^\circ$. A four-point bending specimen configuration shown in Fig. 3 can be reduced to the present problem by cutting it from the middle. By a superposition scheme (Suo and Hutchinson, 1990) and above deformation analysis, the force P and the moment M are

$$P = \frac{P_0 l}{I}\int_0^h (y+H-\delta_3)\,e^{\gamma y}\,dy,$$

$$M = \frac{P_0 l}{I}\int_0^h (y+H-\delta_3)(y-\delta_1)\,e^{\gamma y}\,dy, \tag{33}$$

where

$$I = \int_0^{H+h} (y-\delta_3)^2\,e^{\gamma(y-H)}\,dy. \tag{34}$$

In (33) and (34), δ_3 is the neutral axis of the right side of the plate, and is given by replacing h by $H+h$ in (26). Figure 4 shows that the phase angle and the magnitude of the complex stress intensity factor for the four-point bending specimen. The phase angle varies as γh varies between 0 and 2.4. The variation is larger for smaller h/H, and is quite small when h/H increases to 10. The magnitude of the complex stress intensity factor increases as γh increases, and significantly increases as h/H increases. Figure 5 shows the phase angle and the magnitude of the complex stress intensity of the double-cantilever beam. In this figure,

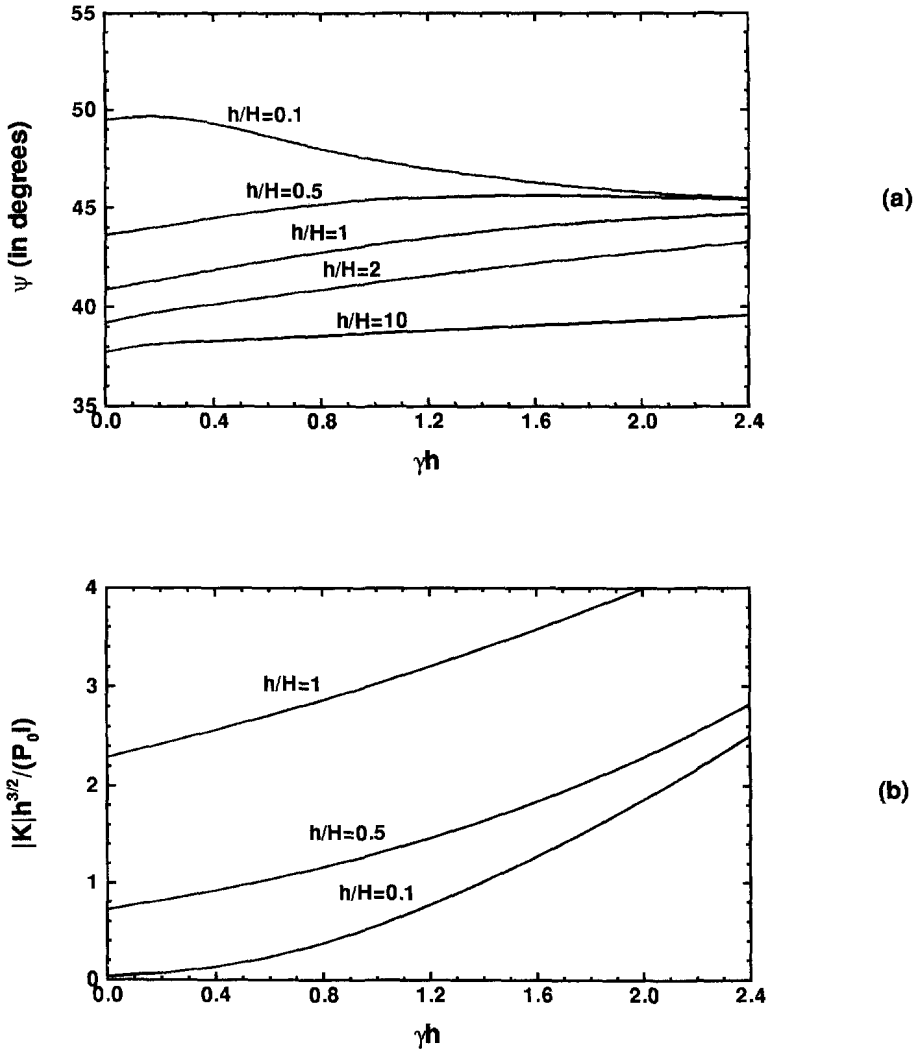

Fig. 4. The phase angle ψ and the magnitude of the complex stress intensity factor $|K|$ for four-point bending specimen.

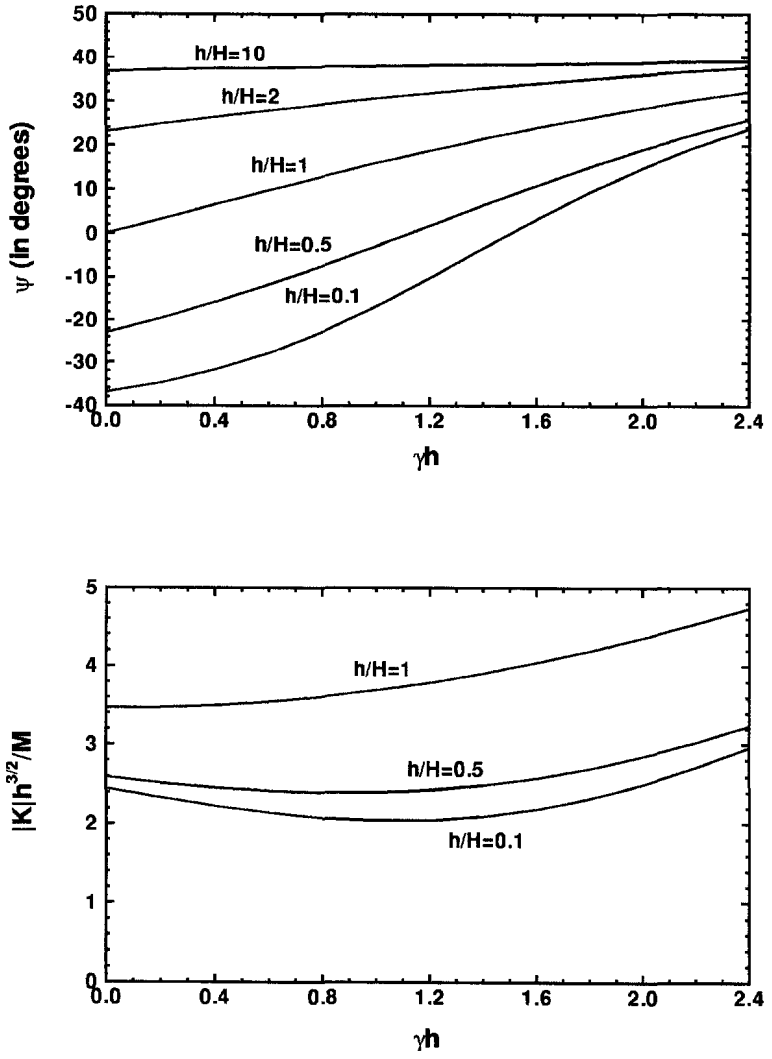

Fig. 5. The phase angle ψ and the magnitude of the complex stress intensity factor $|K|$ for double-cantilever beam.

the phase angle increases as γh or h/H increases. Similar to Fig. 5(a), the variation of the phase angle for γh between 0 and 2.4 is insignificant when h/H increases to 10.

The ratio of the Young's moduli of the two material phases in a FGM, E_u' and E_l', is usually less than 10. From (5),

$$\gamma h = \frac{\ln (E_u'/E_l')}{1 + H/h} \leqslant \ln 10 < 2.4. \tag{35}$$

This tells us that the numerical results for γh between 0 and 2.4 given here provide a complete solution for the semi-infinite crack in FGMs, shown in Fig. 1.

To obtain a quantitative feel for the behavior of the solution, consider the double-cantilever beam (*i.e.*, $P = 0$) with $E_u'/E_l' = 7$. If $h/H = 1$, from (35), $\gamma h \approx 1$. The stress intensity factors are $K_I h^{3/2}/M = 3.55$ and $K_{II} h^{3/2}/M = 1.02$, whereas for a homogeneous material with $h/H = 1$, they are 3.46 and 0, respectively. If $h/H = 0.1$, $\gamma h \approx 0.18$. The stress intensity factors are $K_I h^{3/2}/M = 1.92$ and $K_{II} h^{3/2}/M = -1.34$, whereas for a homogeneous material with $h/H = 0.1$, they are 1.96 and -1.47, respectively. If $h/H = 10$, $\gamma h \approx 1.8$. The stress intensity factors are $K_I h^{3.2}/M = 63.23$ and $K_{II} h^{3/2}/M = 50.71$, whereas for a homogeneous material with $h/H = 10$, they are 62.09 and 46.52, respectively. This shows that the change of K_{II} is larger than that of K_I due to the change of material gradients. Also,

the stress intensity factors at $E'_u/E'_l = 7$ are larger than those of a homogeneous material except the case for $h/H = 0.1$.

For the four-point bending configuration with $E'_u/E'_l = 7$ and $h/H = 1$, the stress intensity factors are $K_I h^{3/2}/(P_0 l) = 2.21$ and $K_{II} h^{3/2}/(P_0 l) = 2.07$; they are 1.73 and 1.50, respectively, for a homogeneous material. If $h/H = 0.1$, the stress intensity factors are $K_I h^{3/2}/(P_0 l) = 0.05$ and $K_{II} h^{3/2}/(P_0 l) = 0.06$; they are 0.03 and 0.03, respectively, for a homogeneous material. If $h/H = 10$, the stress intensity factors are $K_I h^{3.2}/(P_0 l) = 62.79$ and $K_{II} h^{3/2}/(P_0 l) = 51.21$; they are 61.30 and 47.45, respectively, for a homogeneous material. Similar to the double-cantilever beam, the change of K_{II} is larger than that of K_I due to the change of material gradients; and the stress intensity factors at $E'_u/E'_l = 7$ are larger than those of a homogeneous material.

5. SOLUTION FOR ORTHOTROPIC, FUNCTIONALLY GRADED MATERIALS

In this section, we consider the strip in Fig. 1 is made of an orthotropic, functionally graded material. The problem is solved by orthotropy rescaling. In general, there are three material gradients associated with two Young's moduli and one shear modulus. The moduli can be written in following forms

$$\begin{aligned} E'_1(y) &= E_{10}\, e^{\gamma_1 y}, \\ E'_2(y) &= E_{20}\, e^{\gamma_2 y}, \\ \mu_{12}(y) &= \mu(y)\, e^{\gamma_3 y}, \end{aligned} \tag{36}$$

where γ_1, γ_2 and γ_3 are material constants; E_{10} and E_{20} are $E'_1(y)$ and $E'_2(y)$ at $y = 0$, respectively; $\mu_{12}(y)$ is the shear modulus in the x–y plane. For plane stress problems, $E'_1(y) = E_1(y)$ and $E'_2(y) = E_2(y)$, with $E_1(y)$ and $E_2(y)$ being Young's moduli in the directions parallel to the x axis and the y axis, respectively. For plane strain problems, $E'_1(y) = E_1(y)/[1 - \nu_{13}(y)\nu_{31}(y)]$ and $E'_2(y) = E_2(y)/[1 - \nu_{23}(y)\nu_{32}(y)]$, with $\nu_{13}(y)$ and $\nu_{31}(y)$, and $\nu_{23}(y)$ and $\nu_{32}(y)$ being four Poisson's ratios in the x–z and y–z planes, respectively. For isotropic materials, the elastic properties in (36) reduce to those in (1) and (2). The variation of Poisson's ratios can also be written in the exponential form similar to that of the Poisson's ratio in (1) for isotropic materials.

We consider a special set of elastic properties, which is given by

$$\begin{aligned} \gamma_1 &= \gamma_2 = \gamma_3 = \gamma, \\ \nu'_{21}(h) &= \nu_{210}(1 + \varepsilon y)\, e^{\gamma y}, \\ \nu'_{12}(y) &= \nu_{120}(1 + \varepsilon y)\, e^{\gamma y}, \\ \mu_{12}(y) &= \frac{E'_2(y)}{2[\sqrt{\lambda} + \nu'_{21}(y)]}, \end{aligned} \tag{37}$$

whereas ν_{210} and ν_{120} are $\nu'_{21}(y)$ and $\nu'_{12}(y)$ at $y = 0$, respectively; ε is a constant; and

$$\lambda = \frac{E_{20}}{E_{10}}. \tag{38}$$

For plane stress problems, $\nu'_{21}(y) = \nu_{21}(y)$ and $\nu'_{12}(y) = \nu_{12}(y)$, with $\nu_{21}(y)$ and $\nu_{12}(y)$ being two Poisson's ratios in the x–y plane. For plane strain problems, $\nu'_{12}(y) = [\nu_{12}(y) + \nu_{13}(y)\nu_{32}(y)][1 - \nu_{13}(y)\nu_{31}(y)]$, and $\nu'_{21}(y) = [\nu_{21}(y) + \nu_{23}(y)\nu_{31}(y)]/[1 - \nu_{23}(y)\nu_{32}(y)]$. These forms for the material properties of orthotropic, functionally graded materials provide analytical flexibility, and lead to somewhat simple forms for the field equations.

Using this set of elastic properties, the stress function $\Phi(x, y)$ satisfies the following equation

$$\frac{\partial^4\Phi}{\partial x^4}+2\sqrt{\lambda}\frac{\partial^4\Phi}{\partial x^2\partial y^2}+\lambda\frac{\partial^4\Phi}{\partial y^4}-2\gamma\sqrt{\lambda}\frac{\partial^3\Phi}{\partial x^2\partial y}-2\gamma\lambda\frac{\partial^3\Phi}{\partial y^3}+\gamma^2\lambda\frac{\partial^2\Phi}{\partial y^2}=0. \tag{39}$$

Making a variable change

$$x=\lambda^{-1/4}\xi, \tag{40}$$

eqn (39) becomes

$$\frac{\partial^4\Phi}{\partial\xi^4}+2\frac{\partial^4\Phi}{\partial\xi^2\partial y^2}+\frac{\partial^2\Phi}{\partial y^4}-2\gamma\frac{\partial}{\partial y}\left(\frac{\partial^2\Phi}{\partial\xi^2}+\frac{\partial^2\Phi}{\partial y^2}\right)+\gamma^2\frac{\partial^2\Phi}{\partial y^2}=0 \tag{41}$$

in the ξ–y plane. The above equation shows the orthotropy rescaling (Suo *et al.*, 1991) works for nonhomogeneous materials which obey (36) and (37), since it is the same as eqn (3) for isotropic materials. Stresses in terms of $\Phi(\xi, y)$ are

$$\sigma_{xx}=\frac{\partial^2\Phi}{\partial y^2},\quad \lambda^{-1/2}\sigma_{yy}=\frac{\partial^2\Phi}{\partial\xi^2},\quad \lambda^{-1/4}\sigma_{xy}=-\frac{\partial^2\Phi}{\partial\xi\,\partial y}. \tag{42}$$

Stress intensity factors are expressed as

$$\lambda^{-3/8}K_{\mathrm{I}}=\lim_{\xi\to 0,y=0}\sqrt{2\pi\xi}\frac{\partial\Phi}{\partial\xi^2},$$

$$\lambda^{-1/8}K_{\mathrm{II}}=-\lim_{\xi\to 0,y=0}\sqrt{2\pi\xi}\frac{\partial^2\Phi}{\partial\xi\,\partial y}. \tag{43}$$

According to above analysis and the solution for isotropic materials in Section 4, the stress factors to the orthotropic problem are given by

$$\lambda^{-3/8}K_{\mathrm{I}}+i\lambda^{-1/8}K_{\mathrm{II}}=\frac{1}{\sqrt{2}}\left(\sqrt{\frac{A}{h}}P-i\,\mathrm{e}^{i\varphi}\sqrt{\frac{I}{h^3}}M\right)\mathrm{e}^{i\omega}. \tag{44}$$

where A, I, φ and ω are the same as those in the solution for isotropic materials in Section 4.

From above expression, K_{I} and K_{II} are those of the isotropic solution modified by multipliers $\lambda^{3/8}$ and $\lambda^{1/8}$, respectively. The phase angle of the orthotropic problem, ψ_{orth}, relates to that of the corresponding isotropic problem, ψ_{is}, by

$$\tan(\psi_{\mathrm{orth}})=\lambda^{-1/4}\tan(\psi_{\mathrm{is}}). \tag{45}$$

The effects of λ on the crack-tip field depend on its value. When $\lambda>1$, the stress intensity factors are larger than those of the isotropic case, and the phase angle is smaller than that of the isotropic case; and when $\lambda<1$, the stress intensity factors are smaller than those of

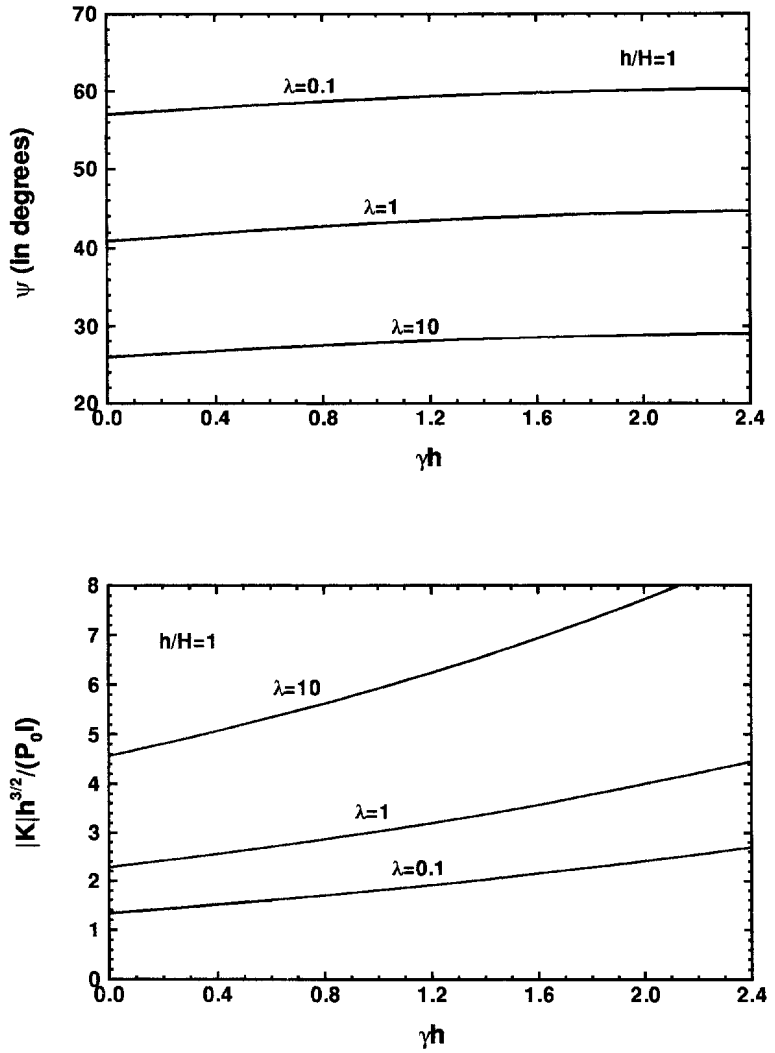

Fig. 6. The effects of λ on the phase angle and the magnitude of the complex stress intensity factor $|K|$ for four-point bending specimen.

the isotropic case, and the phase angle is larger than that of the isotropic case. For the four-point bending specimen configuration, these effects of λ are shown in Fig. 6.

6. THE ANTI-PLANE PROBLEM

The cracked strip shown in Fig. 1 subjected to anti-plane deformation (mode III problem) is considered in this section. For the mode III problem, we take the shear modulus in the following form

$$\mu(y) = \mu_0 \, e^{\gamma y}, \tag{46}$$

where μ_0 is the shear modulus at $y = 0$ and γ represents the material gradient. The strip is loaded at the left side far behind the crack tip, and the traction is

$$\sigma_{xz} = -\sigma_1 \, e^{\gamma y} \tag{47}$$

for $x \to -\infty$ and $y > 0$, and

$$\sigma_{xz} = \sigma_2 \, e^{\gamma y} \tag{48}$$

for $x \to -\infty$ and $y < 0$. The traction produces two uniform strains,

$$\varepsilon_{xz} = -\frac{\sigma_1}{2\mu_0} \tag{49}$$

for $x \to -\infty$ and $y > 0$, and

$$\varepsilon_{xz} = \frac{\sigma_2}{2\mu_0} \tag{50}$$

for $x \to -\infty$ and $y < 0$. From the equilibrium requirement,

$$P = \int_0^h \sigma_{xz} \, dy = \int_{-H}^0 \sigma_{xz} \, dy, \tag{51}$$

and (47) and (48), we have

$$\sigma_1 = \frac{P\gamma}{e^{\gamma h} - 1}, \tag{52}$$

$$\sigma_2 = \frac{P\gamma}{1 - e^{-\gamma H}}.$$

Having the remote field, the stress intensity factor K_{III} is readily obtained from the J integral as

$$K_{III} = \frac{P}{\sqrt{h}} \sqrt{\frac{\gamma h}{e^{\gamma h} - 1} \left(1 + \frac{e^{\gamma h} - 1}{1 - e^{-\gamma H}} \right)}. \tag{53}$$

The normalized stress intensity factor $K_{III}\sqrt{h}/P$, which is equal to the second square root in above equation, is only related to the dimensionless group, γh and γH. It increases as γ increases. When $\gamma = 0$, the stress intensity factor recovers the solution for a homogeneous material; when $\gamma = \infty$ or $H = 0$, it is unbounded. A plot of the stress intensity factor is shown in Fig. 7.

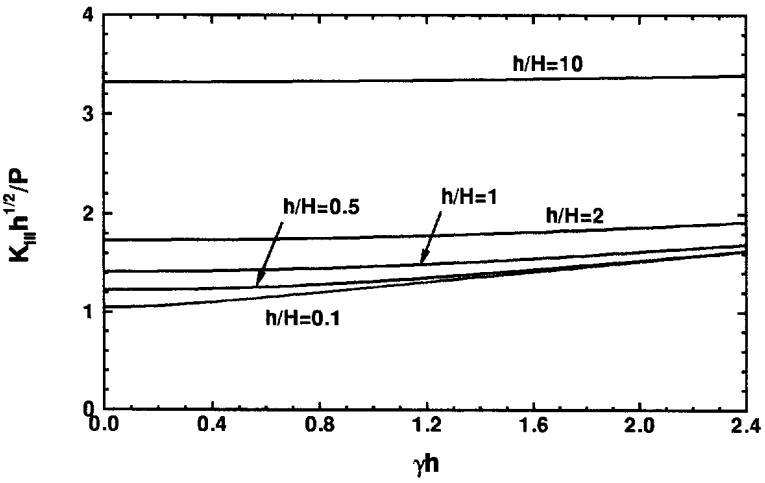

Fig. 7. The stress intensity factor K_{III} for the anti-plane problem.

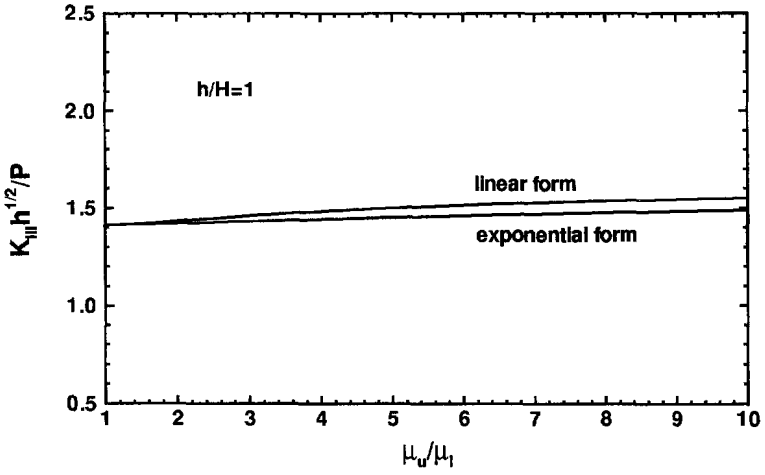

Fig. 8. A comparison of stress intensity factors obtained from different forms of the shear modulus.

When the shear modulus varies linearly along the y axis, it is written as

$$\mu(y) = \frac{\mu_u - \mu_l}{h+H} y + \frac{\mu_u H + \mu_l h}{h+H}, \tag{54}$$

where μ_u and μ_l are shear moduli at the upper and lower boundaries of the strip, respectively. The stress intensity factor for the linear variation of the shear modulus is

$$K_{III} = \frac{P}{\sqrt{h}} \sqrt{\frac{2(r+\eta)}{r\eta+2r+\eta}\left(1+\eta\frac{r\eta+2r+\eta}{r+2\eta+1}\right)}, \tag{55}$$

where $r = \mu_u/\mu_l$ and $\eta = h/H$. A comparison of the stress intensity factor obtained from the linear variation of the shear modulus with that from the exponential variation of the shear modulus is shown in Fig. 8 for $h/H = 1$. The results show that the difference between them is quite small, less than 5% in the range considered. When the crack moves to the ceramic side, the difference between the two solutions becomes smaller, and when it moves to the metal side the difference becomes larger. The difference is less than 0.4% for $h/H = 0.1$; and is less than 8% for $h/H = 10$.

7. DISCUSSION

A complete solution to a semi-infinite crack in a strip of an isotropic, functionally graded material is obtained. It is shown that material gradients have strong effects on the stress intensity factors and the phase angle. For the double-cantilever beam, the mode I stress intensity factor is 3.55 and the mode II stress intensity factor is 1.02, when the crack is at the middle of the strip ($h/H = 1$) and the ratio of the Young's modulus at the upper boundary to that at the lower boundary is 7; for homogeneous material with the same geometry, they are 3.46 and 0, respectively. For the four-point bending specimen configuration, the mode I stress intensity factor is 2.21 and the mode II stress intensity factor is 2.07, when the crack is at the middle of the beam ($h/H = 1$) and the ratio of the Young's modulus at the upper boundary to that at the lower boundary is 7; for a homogeneous material with the same geometry, the two stress intensity factors are 1.73 and 1.50, respectively. These results show that the increase of the mode II stress intensity factor due to the increase of the material gradients is significant, in other words, the mode II stress intensity factor plays an important role in the fracture of FGMs.

The solution for isotropic materials is extended to orthotropic, functionally graded materials by orthotropy rescaling. The effects of the orthotropy on stress intensity factors

and the phase angle are explicitly shown in the orthotropic solution. In the orthotropic solution, since we assume a special set of material properties, the orthotropy is measured by one parameter, the ratio of the Young's modulus in the direction of material property variation to that in the direction perpendicular to the above property variation direction. For general orthotropic, functionally graded materials, there are other parameters in addition to the ratio for characterizing the orthotropy. However, it seems that the ratio is the most important parameter to be considered.

The crack propagation is the competition between the driving force, the energy release rate, and the toughness of the material, *i.e.*, a crack starts to extend when the former one exceeds the latter one. The FGMs are expected to have considerably larger toughness than corresponding bimaterials because there are no large weak planes, such as interfaces, *e.g.*, a layered structure with compositionally graded interlayers is expected to have a larger toughness than that obtained by bonding these layers with sharp interfaces. On the other hand, the energy release rate of a FGM is at the same level as that of the corresponding bimaterial. Consider a bimaterial which has the same configuration as the FGM shown in Fig. 1; above the x axis is material #1 with Young's modulus E'_u and below the x axis is material #2 with Young's modulus E'_l. Figure 9 shows the comparison of the energy release rate of the FGM with that of the bimaterial for the double-cantilever beam when $0 \leqslant h/H \leqslant 2$. In the calculation, $E'_u/E'_l = 7$, and the Poisson's ratios of the two bulk materials forming the bimaterial are taken to be 0.3. For the bimaterial, the two Dundurs' parameters are $\alpha = 0.75$ and $\beta = 0.21$. Our calculation shows, at $h/H = 1$, the energy release rate is 13.55 for the FGM, whereas it is 16.51 for the bimaterial; at $h/H = 0.1$, they are 5.51 and 4.61 for the FGM and the bimaterial, respectively; at $h/H = 10$, they are 6559 and 6517 for the FGM and the bimaterial, respectively. When the crack is at the middle of the plate ($h/H = 1$), the energy release rate of the FGM is smaller than that of the bimaterial; when the crack is very close to the upper or lower boundary, the former one is larger than the latter one. But in any case, the two energy release rates are at the same level. This fact reveals one of the advantages of using FGMs, *i.e.*, FGMs can be subjected to higher external loads than corresponding bimaterials.

The crack propagation direction follows different criteria for different kinds of materials. For homogeneous materials, a crack propagates along the direction in which the mode II stress intensity factor is vanished, and the toughness is independent of the propagation direction and the mode mixity. For bimaterials, the propagation direction of an interface crack is decided by the driving force and the toughness of the interface and the two bulk materials. If the toughness of the bulk materials is relatively large, the interface crack would extend along the interface, otherwise, kinking is favored. For FGMs, their toughness is likely dependent on the material gradients, the position of the crack tip, the

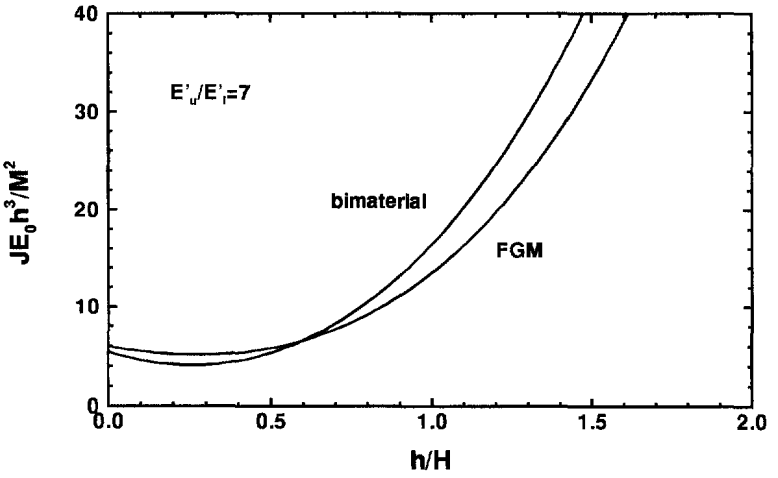

Fig. 9. A comparison of the energy release rate of the FGM with that of the corresponding bimaterial.

propagation direction and the mode mixity. From a continuum point of view, the propagation direction is the direction at which the difference of the energy release rate and the toughness reaches a maximum value, as discussed at the end of Section 3. For complete understanding of the fracture behavior of FGMs and a fully rationalized FGM characterization, experiments need to be carried out and more specimen configurations need to be calibrated.

Acknowledgements—This work is supported by the Office of Naval Research through Grant N00014-93-1-1164.

REFERENCES

Delale, F. and Erdogan, F. (1993). The crack problem for a nonhomogeneous plane. *J. Appl. Mech.* **50,** 609–614.
Delale, F. and Erdogan, F. (1988). On the mechanical modeling of the interfacial region in bonded half-planes. *J. Appl. Mech.* **55,** 317–324.
Dundurs, J. (1969). Edge-bonded dissimilar orthogonal elastic wedges. *J. Appl. Mech.* **36,** 650–652.
Freund, L. B. (1993). The stress distribution and curvature of a general compositionally graded semiconductor layer. *J. Crystal Growth* **132,** 341–344.
Giannakopoulos, A. E., Suresh, S., Finot, M. and Olsson, M. (1995). Elastoplastic analysis of thermal cycling: layered materials with compositional gradients. *Acta Metall.* **43,** 1335–1354.
Holt, J. B., Koizumi, M., Hirai, T. and Munir, Z. A. (eds) (1993). Functionally gradient materials. *Ceramic Transactions*, Vol. 34, The American Ceramic Society, Westerville, OH.
Jin, Z. and Noda, N. (1994). Crack-tip singular fields in nonhomogeneous materials. *J. Appl. Mech.* **61,** 738–740.
Maewal, A., Asaso, R. J. and Dao, M. (1995). Residual stresses in thin film structures with functionally graded materials. In preparation.
Noda, N. and Jin, Z. (1993). Thermal stress intensity factors for a crack in a strip of a functionally gradient material. *Int. J. Solids Structures* **30,** 1039–1056.
Rice, J. R. (1968). A path independent integral and approximate analysis of strain concentration by notches and cracks. *J. Appl. Mech.* **35,** 379–386.
Suo, Z. and Hutchinson, J. W. (1990). Interface crack between two elastic layers. *Int. J. Fract.* **43,** 1–18.
Suo, Z., Bao, G., Fan, B. and Wang, T. C. (1991). Orthotropy rescaling and implications for fracture in composites. *Int. J. Solids Structures* **28,** 235–248.
Thouless, M. D., Evans, A. G., Ashby, M. F. and Hutchinson, J. W. (1987). The edge cracking and spalling of brittle plates. *Acta Metall.* **35,** 1333–1341.
Yamanouchi, M., Koizumi, M., Hirai, T. and Shiota, I. (eds) (1990). *Proceedings of the First International Symposium on Functionally Gradient Materials*, Sendai, Japan.
Yang, W. and Shih C. F. (1994). Fracture along an interlayer. *Int. J. Solids Structures* **31,** 985–1002.